

Research Paper

Radioembolization of Hepatocellular Carcinoma with Built-In Dosimetry: First *in vivo* Results with Uniformly-Sized, Biodegradable Microspheres Labeled with ^{188}Re

José Carlos De La Vega¹, Pedro Luis Esquinas², Cristina Rodríguez-Rodríguez^{1,3}, Mehrdad Bokharraei¹, Igor Moskalev⁴, David Liu⁵, Katayoun Saatchi¹✉, and Urs O. Häfeli¹✉

1. Faculty of Pharmaceutical Sciences, University of British Columbia, Vancouver, BC Canada;
2. Department of Radiology, University of British Columbia, Vancouver, BC Canada;
3. Department of Physics and Astronomy, University of British Columbia, Vancouver, BC Canada;
4. The Vancouver Prostate Cancer Centre and Department of Urologic Sciences, University of British Columbia, Vancouver, BC Canada;
5. Department of Interventional Radiology, Vancouver General Hospital, Vancouver, BC Canada.

✉ Corresponding authors: Urs Häfeli, Katayoun Saatchi; Faculty of Pharmaceutical Sciences, University of British Columbia; 2405 Wesbrook Mall, Vancouver, BC Canada; E-Mail Addresses: urs.hafeli@ubc.ca, kathy.saatchi@ubc.ca.

© Ivyspring International Publisher. This is an open access article distributed under the terms of the Creative Commons Attribution (CC BY-NC) license (<https://creativecommons.org/licenses/by-nc/4.0/>). See <http://ivyspring.com/terms> for full terms and conditions.

Received: 2018.08.21; Accepted: 2019.01.02; Published: 2019.01.25

Abstract

A common form of treatment for patients with hepatocellular carcinoma (HCC) is transarterial radioembolization (TARE) with non-degradable glass or resin microspheres (MS) labeled with ^{90}Y ($^{90}\text{Y-MS}$). To further simplify the dosimetry calculations in the clinical setting, to have more control over the particle size and to change the permanent embolization to a temporary one, we developed uniformly-sized, biodegradable ^{188}Re -labeled MS ($^{188}\text{Re-MS}$) as a new and easily imageable TARE agent.

Methods: MS made of poly(L-lactic acid) were produced in a flow focusing microchip. The MS were labeled with ^{188}Re using a customized kit. An orthotopic HCC animal model was developed in male Sprague Dawley rats by injecting NI-S1 cells directly into the liver using ultrasound guidance. A suspension of $^{188}\text{Re-MS}$ was administered via hepatic intra-arterial catheterization 2 weeks post-inoculation of the NI-S1 cells. The rats were imaged by SPECT 1, 24, 48, and 72 h post-radioembolization.

Results: The spherical $^{188}\text{Re-MS}$ had a diameter of $41.8 \pm 6.0 \mu\text{m}$ ($\text{CV} = 14.5\%$). The site and the depth of the injection of NI-S1 cells were controlled by visualization of the liver in sonograms. Single 0.5 g tumors were grown in all rats. $^{188}\text{Re-MS}$ accumulated in the liver with no deposition in the lungs. ^{188}Re decays to stable ^{188}Os by emission of β^- particles with similar energy to those emitted by ^{90}Y while simultaneously emitting γ photons, which were imaged directly by single photon computed tomography (SPECT). Using Monte Carlo methods, the dose to the tumors was calculated to be 3-6 times larger than to the healthy liver tissue.

Conclusions: $^{188}\text{Re-MS}$ have the potential to become the next generation of β^- -emitting MS for TARE. Future work revolves around the investigation of the therapeutic potential of $^{188}\text{Re-MS}$ in a large-scale, long-term preclinical study as well as the evaluation of the clinical outcomes of using $^{188}\text{Re-MS}$ with different sizes, from 20 to 50 μm .

Key words: radioembolization, liver cancer, microspheres, monosized, ^{188}Re , beta radiation therapy

Introduction

The most common primary cancer of the liver is hepatocellular carcinoma (HCC), which has a poor prognosis with mortality rates close to incidence rates and a 5-year survival rate less than 5% without

treatment [1-3]. Due to delayed detection, size and morphology of the tumor, and poor underlying liver function, only 10% of patients qualify for curative therapies such as ablation, segmental resection, and

transplantation [4-6]. Many patients thus undergo palliative therapies, like transarterial radioembolization (TARE).

In a typical TARE procedure, 20 to 60 μm microspheres (MS) labeled with a radioisotope that emits short-range β^- particles are administered directly into the hepatic artery following optimization of the vascular tree and determination of appropriate activity. In HCC, more than 80% of the blood supply to the tumors is derived from branches of the hepatic artery, whereas the blood supply to the healthy liver tissue is predominately derived from the hepatic portal vein [7, 8]. Due to this uniquely organized dual blood supply to the liver, the MS are preferentially trapped near the terminal arterioles of the tumors resulting in a microembolic effect with little to no hypoxic insult to the liver. As a result, the healthy liver tissue receives less overall radiation, while the tumors are exposed to a tumoricidal radiation dose of 100 to 150 Gy [7, 9].

The most widely utilized TARE agents are TheraSphere[®] (BTG Interventional Medicine; London, United Kingdom) made of glass, and SIR-Spheres[®] (Sirtex Medical Limited; New South Wales, Australia) made of resin [10]. These MS are labeled with ^{90}Y (^{90}Y -MS), which is produced by neutron activation of stable ^{89}Y in a nuclear reactor [11-13]. ^{90}Y decays with a half-life of 64.1 h to stable ^{90}Zr by emission of β^- particles with maximum and mean energies of 2.28 and 0.94 MeV, respectively [14]. When they interact with tissue, these β^- particles generate free oxygen radicals, resulting in cell death. They have maximum and mean penetration distances in tissue of 11.3 and 4.1 mm, respectively. While effective, some ^{90}Y -MS characteristics could be further improved:

- TheraSphere[®] have a size of $25 \pm 10 \mu\text{m}$ [15, 16], while SIR-Spheres[®] have a size of $32.5 \pm 2.5 \mu\text{m}$ [17]. A fraction of the ^{90}Y -MS may bypass the liver and deposit in the lungs due to the arterial/portal shunting of the tumors and the intrinsic sinusoidal pathology in the liver [18].
- ^{90}Y -MS are retained in the patient's capillary bed indefinitely as they are made of non-biodegradable materials, preventing re-opening of the embolized capillaries after treatment [19].
- ^{90}Y -MS are only produced in a few specialized nuclear reactors and they often necessitate long transportation times to the hospital. Therefore, logistics associated with just-in-time manufacturing and delivery across the globe is challenging [20].
- Imaging of ^{90}Y 's β^- particles is not straightforward. The interactions of β^- particles with tissue result in Bremsstrahlung photons which

can be used to create images using single photon emission computed tomography (SPECT). However, such images suffer from poor spatial resolution and limited quantitative accuracy. Alternatively, ^{90}Y can be imaged with positron emission tomography (PET) by exploiting its low-yield internal pair production [21-23], achieving quantitative images that could subsequently be used for dosimetry calculations [24, 25].

- The MS that are labeled with ^{90}Y cannot be labeled instead with a diagnostic radioisotope, such as $^{99\text{m}}\text{Tc}$. To rule out the deposition of MS in undesired organs, patients first undergo a hepatic perfusion study, where macroaggregated albumin (MAA) labeled with $^{99\text{m}}\text{Tc}$ ($^{99\text{m}}\text{Tc}$ -MAA) is administered directly into the hepatic artery [26]. In other words, this hepatic perfusion study simulates a typical TARE procedure. Nonetheless, $^{99\text{m}}\text{Tc}$ -MAA and ^{90}Y -MS do not have the same size and size distribution and $^{99\text{m}}\text{Tc}$ -MAA is prone to disaggregation, potentially leading to misdiagnosis [27, 28].

To address these limitations, we produced uniformly-sized ^{188}Re -labeled MS (^{188}Re -MS). ^{188}Re decays with a half-life of 17.0 h to stable ^{188}Os by emission of β^- particles with maximum and mean energies of 2.12 and 0.76 MeV, respectively [29]. These β^- particles have a maximum and a mean penetration distance in tissue of 11.0 and 3.8 mm, respectively, very similar to those of ^{90}Y [30]. At the same time, ^{188}Re emits 155 keV γ photons with an abundance of 15.6%, allowing for *in vivo* imaging by SPECT for patient-specific dosimetry calculations and biodistribution studies [31-35]. Timing and transportation issues may be mitigated due to the generator-based production of ^{188}Re from the decay of ^{188}W , which has a half-life of 69.4 days. The $^{188}\text{W}/^{188}\text{Re}$ generator is a continuous source of no-carrier-added ^{188}Re for at least 4 to 6 months [36-38] and can be conveniently placed in hospitals, allowing for on-site ^{188}Re labeling of the MS with the exact prescribed activity at the time of need [37, 39].

In summary, $\sim 40 \mu\text{m}$ MS were produced using a microfluidic technology, labeled with ^{188}Re , administered into two HCC-bearing rats (Cohort A, HCC/+) and two healthy rats (Cohort B, HCC/-), and imaged by SPECT. This small-scale pilot study had the following two objectives: 1) to garner preliminary data of the biodistribution of the ^{188}Re -MS and 2) to develop an algorithm to estimate the radiation doses to the tumor and the healthy liver tissue using SPECT images.

Material and methods

Animals

The study was conducted in accordance with the guidelines of the Canadian Council on Animal Care and the protocol approved by the Animal Care Committee of the University of British Columbia in Vancouver, Canada (A15-0244). Four ~250 g male Sprague-Dawley rats were purchased from Charles River Laboratories (Wilmington, Delaware, United States) and housed at the Modified Barrier Facility and the Centre for Comparative Medicine at the University of British Columbia. The rats were provided with food and water *ad libitum*. This small sample size was used to garner preliminary data to support future research and refine two complex surgical techniques: the ultrasound-guided injection of tumor cells into the liver and the administration of ^{188}Re -MS via a hepatic intra-arterial catheterization.

Production, radiolabeling, and characterization of ^{188}Re

The MS were produced using a microfluidic chip with a flow focusing configuration. In a flow focusing microchip, a polar continuous phase flows through two outer microchannels and meets a non-polar dispersed phase at an inner microchannel, where the dispersed phase is squeezed until it breaks into uniform and size-defined spherical droplets (Figure 1A). After an evaporation step, the droplets harden and become microspheres [40-42].

The MS were made of a blend of three polymers: 1) commercially available poly(L-lactic acid) (*L*-PLA) (2.2 kDa; Resomer[®] L104, Boehringer Ingelheim; Burlington, Ontario, Canada), 2) a custom-synthesized chelating polymer for ^{188}Re labeling (or ^{188}Re chelomer), and 3) MePEG_{17-b}-PCL₁₀ (or PEG-PCL; a PEGylated polycaprolactone added to prevent

aggregation of the MS in water). The chelomer used herein was previously reported by Saatchi *et al.* (2007) and it is constituted of *L*-PLA chains capped with bis(picoly)amine, a tridentate ligand that binds ^{188}Re [43].

The MS were produced in the microchip fabricated and previously reported by Bokharai *et al.* (2016) (Figure 1B) [40]. A 2% w/v poly(vinyl alcohol) (PVA; 13-23 kDa, 87-89% hydrolyzed, Sigma Aldrich; Oakville, Ontario, Canada) solution was prepared as the continuous phase. The sterile-filtered solution was withdrawn into two 10 mL glass syringes and pumped into the microchip at a flow rate of 30 $\mu\text{L}/\text{min}$. A 5% w/v solution in chloroform of the polymer blend described before was prepared as the dispersed phase. The concentrations of the three polymers in the blend were: 1) 87% w/w *L*-PLA, 2) 10% w/w ^{188}Re chelomer, and 3) 3% w/w PEG-PCL. After mixing well, this solution was withdrawn into a 1 mL glass syringe and it was pumped into the microchip at a flow rate of 1 $\mu\text{L}/\text{min}$.

The breakup of the stream into droplets was monitored using an inverted microscope (AE31, Motic; Kowloon, Hong Kong, China) equipped with a digital camera (Moticam 3, Motic; Kowloon, Hong Kong, China). The collection of the droplets began only after the two phases had been pumping for 20 min and the flow was judged to be stable by visual inspection. The sample of MS was collected for 420 min in a 20 mL glass vial with 4 mL of the 2% w/v PVA solution. After evaporation of chloroform, the sample was washed with water six times to remove traces of PVA, lyophilized (FreeZone[®], Lonza; Basel, Basel-Stadt, Switzerland), and stored at 4 °C until needed.

A $^{188}\text{W}/^{188}\text{Re}$ generator (ITM Isotopen Technologien München AG; Garching, Bavaria, Germany) was utilized as the source of $[\text{}^{188}\text{ReO}_4]^-$, which was eluted as $\text{Na}^{188}\text{ReO}_4$ using saline.

To label the MS with ^{188}Re , a customized ^{188}Re labeling kit was prepared to reduce $[\text{}^{188}\text{ReO}_4]^-$ to $[\text{}^{188}\text{Re}(\text{H}_2\text{O})_3(\text{CO})_3]^+$ under vacuum using a Schlenk line. For the reaction, potassium boronocarbonate (Dalton Pharma, Toronto, Canada) was used as both a reducing agent and an *in situ* source of CO [44]. Following a procedure reported by Saatchi *et al.* (2009) to label similar MS with $^{99\text{m}}\text{Tc}$, ^{188}Re 's congener, $[\text{}^{188}\text{Re}(\text{H}_2\text{O})_3(\text{CO})_3]^+$ was added to a 20 mg/mL suspension of MS in water. The activity of $[\text{}^{188}\text{Re}(\text{H}_2\text{O})_3(\text{CO})_3]^+$ added was 67.7 MBq per mg of MS. The mixture was incubated at 70 °C for 30 min in a

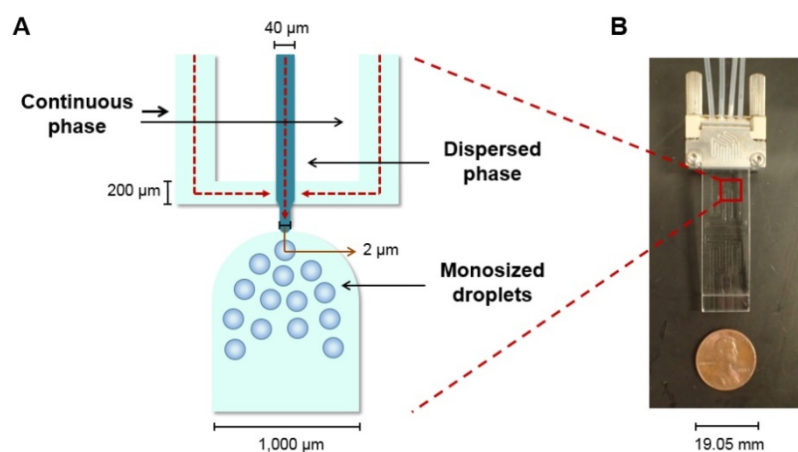


Figure 1. Flow focusing microchip. (A) Schematic of the microchip's flow focusing configuration with the directions of the flows indicated with red arrows. (B) Image of the microchip utilized to produce the MS described in this manuscript.

Thermomixer R (Eppendorf; Mississauga, Ontario, Canada) shaking at 500 rpm. The ^{188}Re -MS were then allowed to precipitate for at least 15 min, the supernatant was removed, and the ^{188}Re -MS were suspended in 50 μL of saline [45].

Binding of $^{188}\text{Re}(\text{CO})_3^+$ was corroborated by thin layer chromatography (TLC) using saline as the mobile phase. The labeling efficiency was calculated by dividing the total activity minus the activity of the supernatant by the total activity. All activity measurements were taken using a liquid scintillation counter (Tri-Carb 4910TR, Perkin Elmer; Waltham, Massachusetts, United States).

The size distribution of the MS before $^{188}\text{Re}(\text{CO})_3^+$ binding was determined using a microsphere-based method. The MS were suspended in water at a concentration of 1 mg/mL. A 20 μL aliquot of this suspension was pipetted onto a glass microscope slide and imaged by brightfield microscopy (AE31, Motic; Kowloon, Hong Kong, China). The diameters of 500 MS in many images were measured using ImageJ [46].

The external morphology of the MS was inspected by scanning electron microscopy (SEM; SU3500, Hitachi; Chiyoda, Tokyo, Japan), before $^{188}\text{Re}(\text{CO})_3^+$ binding and after ^{188}Re decay. The MS were suspended in water at a concentration of 1 mg/mL. For both suspensions, a 20 μL aliquot was pipetted onto specimen stubs covered with an electrically conductive carbon-based adhesive disc. The specimen stubs were dried in a purifier vertical clean bench (37400-01, Labconco; Kansas City, Missouri, United States) for 8 h. They were then sputter-coated with an 8 nm layer of iridium using a modular high vacuum coating system (EM MED020, Leica; Wetzlar, Hesse, Germany) under reduced pressure (<5 Pa). The images were acquired at 15 kV with a magnification of 1,000x.

Development of a hepatocellular carcinoma-bearing animal model

HCC was induced in the two rats allocated to Cohort A (HCC/+) by injecting them directly into the liver with a suspension of N1-S1 cells (ATCC[®] CRL-1604[™]; Manassas, Virginia, United States). N1-S1 cells proliferate and form a highly chemoresistant tumor known as Novikoff HCC [39], which mimics the resistance often seen in human HCC [47]. The two rats allocated to Cohort B (HCC/-) received an injection of saline.

Preparation of injections of N1-S1 cells

The N1-S1 cells were cultured in suspension at 37 °C and 5% CO_2 in Iscove's Modified Dulbecco Medium (IMDM; ThermoFisher Scientific; Waltham, Massachusetts, United States) supplemented with

10% w/v fetal bovine serum (FBS; ThermoFisher Scientific; Waltham, Massachusetts, United States) and 1% w/v penicillin-streptomycin, or simply Pen-Strep (10,000 U mL^{-1} , ThermoFisher Scientific; Waltham, Massachusetts, United States). For each rat, an injection of 1×10^6 N1-S1 cells was prepared in a 1 mL syringe connected to a 30G 1" needle. This number of N1-S1 cells has been reported to form a ~0.5 to 1 g tumor 2 weeks post-inoculation [39, 48].

The N1-S1 cells were suspended in 50 μL of Corning[™] Matrigel[™] Membrane Matrix (Matrigel[™] for short; Fischer Scientific; Hampton, New Hampshire, United States). Matrigel[™] is a mixture of proteins that polymerizes irreversibly at room temperature, becoming a stable and effective matrix for the attachment of cells [49-51]. The syringes were kept on ice to avoid polymerization of the suspension of N1-S1 cells before injection.

Ultrasound-guided inoculation of N1-S1 cells into the liver

The inoculation of N1-S1 cells was performed via an ultrasound-guided percutaneous injection using the Vevo[®] 2100 Digital Imaging Platform (Visual Sonics; Toronto, Ontario, Canada). A 40 MHz ultra-high frequency transducer, also from Visual Sonics, was utilized to visualize the liver and inject the suspensions of N1-S1 cells in Matrigel[™] directly below the capsule of the left lobe of the liver.

The two rats allocated to Cohort A (HCC/+) were anesthetized with isoflurane on a precision vaporizer (5% v/v oxygen for induction, 1.5 to 2.5% v/v oxygen for maintenance) and they received a subcutaneous injection of 3 to 5 mL of lactated Ringer's solution for hydration. They were mounted in a supine position on the machine's heated operating table with continuous monitoring of vital signs. As preemptive analgesia, 1 mg/kg SQ meloxicam was administered. The abdomen was shaved, disinfected with 0.5% w/v chlorhexidine solution (Stanhexidine[®], Omega Laboratories Limited; Montreal, Quebec, Canada), and fully covered with a thin layer of ultrasound gel (Aquasonic[®], Parker Laboratories Inc.; Fairfield, New Jersey, United States). The liver was visualized on the machine's screen. The syringe filled with the cell suspension was brought to the skin just below the rib cage at an angle of 20 to 40° with the bevel up. After detection of the needle on the machine's screen, the needle was passed through the skin and the abdominal wall muscles and directed underneath the liver capsule. The suspension was injected slowly into the left lobe. After a 3 s pause to prevent leakage of the suspension, the needle was rapidly withdrawn. The rats were immediately recovered.

The same procedure was conducted in the two rats allocated to Cohort B (HCC/-) to administer 50 μL of saline directly into the left lobe of the liver, underneath the capsule.

Transarterial radioembolization and quantitative SPECT

A hepatic intra-arterial catheterization was performed in all rats 2 weeks after receiving an injection of N1-S1 cells (Cohort A; HCC/+) or saline (Cohort B; HCC/-). The rats in Cohort A are referred to as R01 and R02, whereas the rats in Cohort B are referred to as R03 and R04.

Preparation of injections of $^{188}\text{Re-MS}$

A parenteral formulation was developed by suspending the $^{188}\text{Re-MS}$ in a sterile solution made of 1.75% w/v hydroxyethyl cellulose (24-27 kDa, Polysciences Inc.; Warrington, Pennsylvania, United States), 5% w/v dextrose (Baxter International Inc., Deerfield, Illinois, United States), and 0.01% w/v Chicago Sky Blue 6B (Sigma Aldrich; Oakville, Ontario, Canada) (or “HEC/Dex/CSB”, for short). The hydroxyethyl cellulose was used as a viscosity enhancer, the dextrose was used as a tonicity agent, and the Chicago Sky Blue 6B, which is a dye, was simply added to facilitate the visualization of the $^{188}\text{Re-MS}$ during administration. The viscosity of the HEC/Dex/CSB solution was determined to be 5.6 ± 0.2 cP at body temperature using a rotational rheometer (MCR 301, Anton Paar; Graz, Styria, Austria). Therefore, it is six times more viscous than water and three times more viscous than blood [52]. The osmolality was determined to be 289.5 ± 2.1 mOsm/kg using a vapor pressure osmometer (VAPRO®, EliTech Group; Puteaux, Île-de-France, France).

For each rat, a vascular catheter made of polyethylene (PE-50, ID = 0.05 cm and OD = 0.10 cm, Intramedic™, Becton Dickinson; Franklin Lakes, New Jersey, United States) was customized to administer the $^{188}\text{Re-MS}$ with minimal losses in the needles, syringes, and catheters. One end of a 20 cm long PE-50 catheter (referred to as “Catheter 1”) was stretched so that its final size was approximately equal to that of a PE-10 catheter (ID: 0.02 cm, OD: 0.05 cm). This was accomplished with the help of a heat gun, which was placed approximately 30 cm away from the catheter. The catheter was stretched by twisting and pulling it simultaneously while applying heat. The tip of the catheter was cut at a 45° angle with a razor blade to facilitate insertion into the rat. The stretched section was approximately 5 cm long.

The unaltered end of Catheter 1 was coupled to a 1 mL syringe filled with 500 μL of saline and

connected to a 23G 1” blunt needle (referred to as “Syringe A”). A 100 cm long PE-50 catheter (referred to as “Catheter 2”) was connected to a 1 mL syringe filled with 200 μL of saline (referred to as “Syringe B”) and was placed inside a 3 mm thick box made of poly(methyl methacrylate) to shield the β^- emissions of ^{188}Re . This system was then put inside a lead container to shield the γ emissions of ^{188}Re from one side (Figure 2). A 1 cm thick sheet of lead was placed on the other side of the container to shield the γ emissions from the other side.

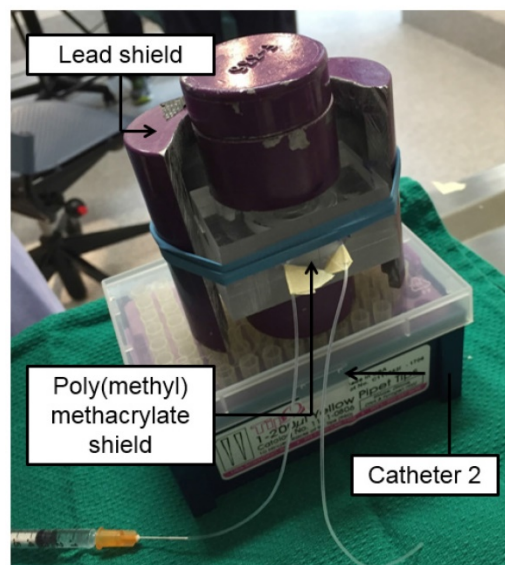


Figure 2. Setup for administration of ^{188}Re -labeled microspheres. The poly(methyl methacrylate) shield contains the β^- emissions of ^{188}Re , while the lead shield protects the user from the γ emissions of ^{188}Re . Catheter 2 contains the pre-loaded suspension of $^{188}\text{Re-MS}$ fully shielded within the poly(methyl methacrylate) box.

Table 1 summarizes the number of $^{188}\text{Re-MS}$ and the activity injected in each rat. The activity was measured using a CRC®-55tR dose calibrator (Capintec; Florham Park, New Jersey, United States). The dose calibrator settings for ^{188}Re were determined experimentally using the method described in [32]. The $^{188}\text{Re-MS}$ were suspended in 100 μL of the HEC/Dex/CSB solution. This suspension was withdrawn into Catheter 2, followed by 50 μL of saline. The catheter is long enough to contain this volume without drawing the $^{188}\text{Re-MS}$ into the syringe, preventing losses during their administration. A polished 1 cm long piece of a 23G blunt needle was then inserted into the free end of Catheter 2. This assemble is referred herein as the 23G/Catheter 2/Syringe B system. This technique was developed and previously reported by Häfeli *et al.* (1999) [39]. A schematic of the set of catheters and syringes can be found in Figure 2 of the manuscript just referenced.

Table 1. Activity of ^{188}Re -labeled microspheres per rat.

Cohort ID	Animal ID	Number of ^{188}Re -MS	Activity (MBq)	Specific activity (Bq per MS)	Activity measured on SPECT (MBq)
Cohort A (HCC/+)	R01	47,700	44.4	945	50.3
	R02	47,700	12.6	238	13.8
Cohort B (HCC/-)	R03	71,600	55.5	782	56.5
	R04	47,700	11.5	245	12.1

The rats received an injection of 2 mg (R01, R02, and R04) or 3 mg (R03) of ^{188}Re -MS via a hepatic intra-arterial catheterization 2 weeks post-inoculation of 1×10^6 N1-S1 cells (Cohort A; HCC/+) or saline (Cohort B; HCC/-) into the left lobe of the liver. Each cohort received an injection of high and low specific activity.

Hepatic intra-arterial catheterization

The suspension of ^{188}Re -MS in HEC/Dex/CSB was administered directly into the proper hepatic artery (PHA), which provides the tumor with most of its blood supply. The PHA arises from the common hepatic artery (CHA) and, together with the hepatic portal vein and the common bile duct, forms part of the portal triad. The portal triad is a distinctive group of blood vessels in the liver. TARE with ^{188}Re -MS was accomplished by performing a laparotomy followed by a hepatic intra-arterial catheterization.

The rats were anesthetized with isoflurane and mounted in a supine position on a heated operating table with continuous monitoring of vital signs. The abdomen was shaved and disinfected with 0.5% w/v chlorhexidine solution (Stanhexidine®, Omega Laboratories Limited; Montreal, Quebec, Canada) and 70% w/v isopropyl alcohol. As a local anesthetic, 8 mg/kg of a 0.25% w/v bupivacaine solution was injected on the incision site, between the right and the left upper quadrants of the abdomen. A laparotomy was then performed and the left lateral lobe of the

liver was externalized and retracted using a piece of gauze soaked with saline and held back by needle holders. Cotton tipped applicators were used to gently dissect through the mesentery to expose the portal triad after pushing the first loop of the duodenum caudally. A clean cotton-tipped applicator was utilized to clear the portal triad of excess connective tissue and expose the following blood vessels: PHA, CHA, and gastroduodenal artery (GDA). To prevent bleeding in the event of puncture, the CHA was temporarily ligated with a removable micro bulldog clamp. A small curved hemostat was used to isolate the GDA. To control retrograde bleeding, the GDA was ligated with a 4-0 suture close to the branch point with the posterior pancreatoduodenal arcade. A 2-0 suture beneath the GDA was utilized to apply tension on the blood vessel during the catheterization (Figure 3).

A surgical microscope (M525 F20, Leica; Wetzlar, Hesse, Germany) was used to insert the stretched end of Catheter 1 into the GDA proximal to two ligation sites, but as distally to the branch point of the GDA from the CHA as possible. While maintaining tension on the 2-0 suture under the GDA, the catheter was carefully advanced into the CHA, placing the tip in the common branch with the PHA. The catheter was then fixed in place with a 2-0 suture. The knot was placed proximal to the insertion site to prevent bleeding and hold the catheter tightly within the wall of the PHA without occluding the lumen. When Catheter 1 was secured at the injection site, Syringe A was exchanged with the 23G/Catheter 2/Syringe B system. The suspension of ^{188}Re -MS was then injected in a slow and controlled fashion.

The previously externalized liver lobe was returned to the abdominal cavity. To restore hemodynamics, 100 μL of heparin lock flush and 500 μL of saline were infused. After removal of Catheter 1, the two ligation sites were repaired with 2-0 sutures and the presence of appropriate blood flow to the liver was confirmed. The body wall and skin were closed with 5-0 sutures with simple and continuous subcutaneous patterns, respectively.

All sutures were made with Coated VICRYL® (Ethicon, Inc.; Bridgewater, New Jersey, United States). The rats received a split dose of buprenorphine (i.e., half dose pre-op and half dose post-op; Total Dose = 0.05 mg/kg). Upon recovery, they all continued on 0.01 to 0.05 mg/kg buprenorphine. The dose was

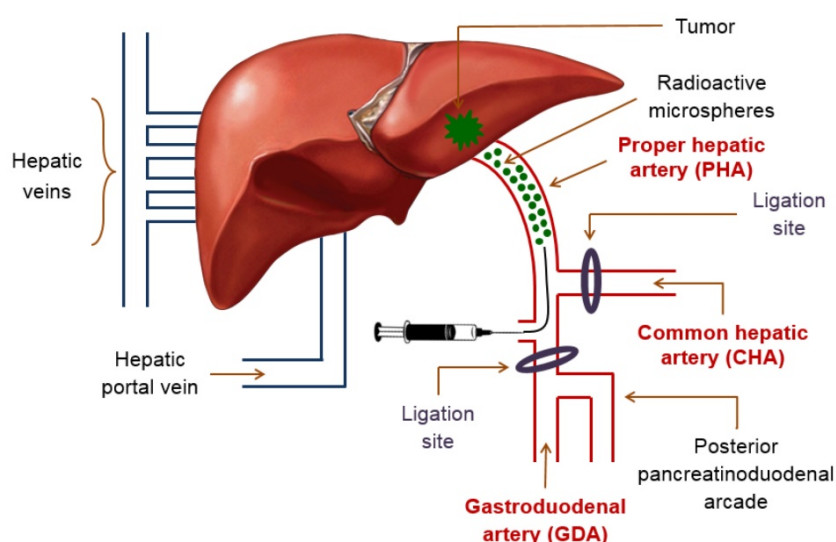


Figure 3. Schematic of the hepatic intra-arterial catheterization. The cartoon depicts the most important blood vessels involved in the surgery performed for administration of ^{188}Re -MS into the liver. Access to the PHA was gained through the GDA. During the surgery, blood flow in the CHA was temporarily stopped in the CHA with a micro bulldog clamp and in the GDA with a 4-0 suture. These two ligation sites were repaired after administration of the ^{188}Re -MS to ensure appropriate blood flow to the liver.

determined on a case-by-case basis based on the degree of pain signs. Furthermore, 1 mg/kg meloxicam was administered if deemed necessary following a clinical assessment. All analgesics were administered subcutaneously.

Quantitative SPECT

Still under general anesthesia from the surgery described above, the rats were imaged using the VECTor Imaging Platform (MILabs; Utrecht, Utrecht, Netherlands), a preclinical SPECT/PET/CT system (where PET and CT stand for positron emission tomography and computed tomography, respectively). Taking into account the time required to close the sutures and stabilize the vital signs of the rats, the scans were performed approximately 1 h post-radioembolization. For two of the rats, R01 and R03, additional SPECT/CT scans were performed 24, 48, and 72 h post-radioembolization to investigate changes in the localization of the ^{188}Re -MS after administration and to determine the effective half-life of the ^{188}Re MS in the liver.

The rats were placed on a heating pad during the scans with continuous monitoring of vital signs. The SPECT scans were performed with the Ultra-High Resolution Collimator (UHRC) by MILabs (Utrecht, Utrecht, Netherlands), a rat size multi-pinhole collimator with the a bore diameter of 98 mm, a wall thickness of 15 mm, a pinhole diameter of 1 mm, and a total number of pinholes of 75 [32]. The scan time was increased for the later time point scans to maximize the counts and minimize the noise, but taking into account the time that the rats could remain safely under anesthesia. For example, the scan time was 30 min for the scans conducted 1 h post-radioembolization, 60 min for the scans conducted 24 and 48 h post-radioembolization, and 90 min for the scans conducted 72 h post-radioembolization. Following each SPECT scan, a whole-body CT scan was acquired to obtain anatomical information of the rats and create a transmission map which was utilized for attenuation correction. Both images were subsequently registered.

The ^{188}Re photopeak window was centered at 155 keV with a 20% energy window width. For quantitative analysis, SPECT image reconstructions were carried out with a pixel-ordered subset expectation maximization (POSEM) algorithm that included resolution recovery and compensation for distance-dependent pinhole sensitivity. For the SPECT images, we used 16 subsets, 16 iterations, and an isotropic 0.4 mm voxel grid. All images were corrected for decay, attenuation, and scatter, which was accomplished with the triple-energy window method [53]. In order to relate the units of the scanner

(counts per pixel) to radioactivity concentration (MBq per mL), a calibration factor was determined by scanning a source with a known concentration of ^{188}Re . The overall details of this image reconstruction protocol and the assessment of activity quantification accuracy of ^{188}Re SPECT in VECTor Imaging Platform (MILabs; Utrecht, Utrecht, Netherlands) was described previously [32].

For visual representation, the reconstructed volumes of the SPECT scans were post-filtered with a three-dimensional (3D) Gaussian filter. CT scans were acquired at 45 kV and 615 μA . In total, two frames of 180 projections over 360° were acquired in a step-and-shoot rotation mode. The acquired projection data was reconstructed using SkyScan NRecon software to generate a 3D CT image with a 0.169 mm³ voxel size.

Dosimetry calculations

Accurate image-based dosimetry calculations of radionuclide therapies require the following information: 1) the cumulated activity distribution (i.e., the total number of disintegrations of the radioisotope in the region of interest [ROI]), 2) the energy deposited by the radioisotope's emissions in the tissue (per unit decay), and 3) the boundaries of the ROI (i.e., segmentation of the tumor and the liver). While ^{188}Re SPECT images on the VECTor Imaging Platform (MILabs; Utrecht, Utrecht, Netherlands) are quantitatively accurate [32] and can be utilized to determine the cumulated activity in the ROIs, the limited resolution and the low contrast difference in the CT images of the rats did not allow us to distinguish with confidence the boundaries of the tumor and the healthy liver tissue. For this reason, we estimated the doses to the tumor and the healthy liver tissue using a simplified approach. Our approach made use of the tumor-to-healthy liver activity concentration ratio (T/H) (derived from the quantitative SPECT images), the measured administered activity, the masses of the tumor and the liver (determined *ex-vivo*) and a two-compartment liver-tumor model. The details of our method, which were applied to all the animals included in our study, are described below.

First, using AMIDE (v.1.0.5), the T/H was estimated from the SPECT images of the animals by calculating the ratio of the mean voxel intensity in the tumor region to the mean voxel intensity in the healthy liver tissue. These regions were approximated from an *ex vivo* analysis of the livers of the rats. The mean voxel intensities were determined by drawing spherical VOIs on the SPECT image. The number of VOIs was selected to cover the complete volume of the target regions uniformly. For example, up to three

VOIs with 0.68 mm in diameter were required for the tumor, but eight VOIs with 1.69 mm in diameter were required for the healthy liver tissue.

Second, a simplified voxelized geometry (i.e., voxel size equal to that of the SPECT images) representing the anatomy of the liver and the tumor was created. The liver geometry was modeled as a sphere with uniform soft tissue density and a volume equal to that of the rat's liver (determined from *ex-vivo* measurements of its mass). Similarly, the tumor was modeled as a sphere placed within the liver, off-center. The masses of the livers and the tumors were between 11.8 and 15.4 g and 0.4 and 0.6 g, respectively. The voxelized liver-tumor maps were converted into activity maps, in MBq, by assuming that the activity administered was uniformly distributed in the liver and tumor volumes, taking into consideration the T/H ratio derived from the SPECT images.

Third, to convert the activity maps into cumulated activity maps, the relative change of activity as a function of time in the liver was derived from the SPECT images at each time point. In particular, for each time point, the average voxel value within a VOI enclosing the liver region was measured. Subsequently, a mono-exponential function was fitted to these data and the effective half-life of the ^{188}Re -MS (T_{eff}) was derived. The cumulated activity (\tilde{A}_i) in each voxel i of the geometry was then determined with the following expression:

$$\tilde{A}_i = A_{0,i} \int_{t=0}^{t=\infty} e^{-\frac{\ln(2)t}{T_{eff}}} dt = A_{0,i} \times \frac{T_{eff}}{\ln(2)} \quad (\text{Equation 1})$$

Finally, the dose map was determined by convolving the cumulated activity map with a ^{188}Re point-dose kernel. The dose kernel, which represents the amount of dose deposited by a point-source of ^{188}Re per disintegration in a uniform density voxelized medium, was determined by means of Monte-Carlo simulations using Geant4 Applications for Computed Tomography v7.1 (GATE) [54]. More specifically, 10^7 decays of ^{188}Re were simulated in the voxelized medium and the energy deposited per voxel (and therefore, the dose) was scored. The ^{188}Re decay data was built-in in GATE and is based on the Evaluated Nuclear Structure Data File (ENDSF) database [55]. The physics models included photoelectric effect, Compton and Rayleigh scattering, pair production, electron ionization and scattering, Bremsstrahlung and electron-positron annihilation.

The final radiation dose absorbed by the tumor and the healthy liver tissue was computed by averaging the dose-map values within the spherical tumor and the healthy liver tissue (i.e., the volume of the entire liver minus the volume of the tumor).

Histology

All rats were sacrificed via transcatheter perfusion following the last SPECT/CT scan. To show the microembolic effect of the ^{188}Re -MS, a sample of the PHA was collected, stored in formalin, and sent out to Wax-It Histology Services Inc. for tissue processing and histology. Specifically, the tissue was embedded into a paraffin-block. Using a microtome, 50 μm sections were cut and mounted onto microscope slides for imaging and analysis.

Results and discussion

Production, radiolabeling, and characterization of the microspheres

Our microfluidic chip is a versatile technology that allows for the production of quasi-monosized MS with different sizes. We can produce MS with a diameter between 20 and 50 μm , which is also the range of sizes of ^{90}Y -MS, simply by varying the concentration of the polymer blend in the dispersed phase and the flow rates of the continuous and the dispersed phases. For example, Figure 4 shows samples of ~ 20 , ~ 30 , ~ 40 , and ~ 50 μm MS produced using the same microfluidic chip. All of these samples have a coefficient of variation (CV) below 16%, which, based on the monodispersity criterion of the National Institute of Standards and Technology (NIST), means they are quasi-monosized [56, 57]. We worked with ~ 40 μm MS made of a blend of 87% w/w L-PLA, 10% w/w ^{188}Re -chelomer, and 3% w/v PEG-PCL for the next stages of this study. These MS had a diameter of 41.8 ± 6.0 μm with a narrow size distribution ($CV = 14.5\%$). Using SEM, we verified that the MS were spherical and they preserved their size and shape after labeling with ^{188}Re (Figure 5). These characteristics make them a suitable TARE agent.

Figure 6A shows a schematic of the ^{188}Re labeling procedure. The exact number of ^{188}Re chelators on the surface of the MS is unknown, as the ligand is quite lipophilic and many chelating groups will thus be inside the MS and not accessible for labeling. The MS were functionalized with $[\text{Re}(\text{CO})_3]^+$ with a labeling efficiency of 50 to 80% across different batches. The MS were labeled in the absence of oxygen to prevent oxidation of $[\text{Re}(\text{CO})_3]^+$ back to $[\text{ReO}_4]^-$, which does not bind to the surface of the MS [45]. To increase the labeling efficiency and reduce the variability from batch to batch, we are currently working on evaluating the effect of variables such as time, temperature, reaction volume, and activity concentration on the labeling of the MS with ^{188}Re . Figure 6B compares the TLC of the ^{188}Re -MS to that of free, or unbound, $[\text{Re}(\text{CO})_3]^+$. ^{188}Re -MS stay at $R_f = 0$, while free $[\text{Re}(\text{CO})_3]^+$ moves to $R_f = 1$. Before injection into the

rats, free $[^{188}\text{Re}(\text{CO})_3]^+$ was fully removed by allowing the MS to settle, removing the supernatant, and washing them with water six times. Hence, a known number of clean, radiolabeled MS was injected into each rat.

Our technique for labeling the MS with ^{188}Re allows for the production of ^{188}Re -MS with different specific activities. For example, Table 1 shows that ^{188}Re -MS with specific activities between 245 and 945 Bq per MS were produced and injected into the rats. The specific activity depends on the activity used to label the MS as well as the number of MS in the sample, but it can also be increased or decreased by varying the concentration of the chelomer for ^{188}Re binding in the formulation. This yields an advantage over ^{90}Y -MS, which are produced with the following pre-defined specific activities: 2.5 kBq and 40 Bq per

MS for TheraSphere® and SIR-Spheres®, respectively [20]. In the clinical setting, our formulation thus has the potential of easily adjusting both the activity and the number of MS on a per patient basis.

Our uniformly-sized ^{188}Re -MS constitute one of the first efforts to produce a ^{188}Re -labeled radioembolization agent made of a blend of fully biodegradable polymers. Current radioembolization agents are retained in the patient's capillary bed indefinitely due to their non-biodegradable nature, thus preventing reopening of the clogged capillaries after radioembolization [58-60]. Once lodged in the capillaries, the polymer chains in the ^{188}Re -MS will slowly break down into smaller polyester fragments, which will be absorbed and recycled by the body in the form of lactic acid. This process can take up to 3 to 6 months at 37 °C [61].

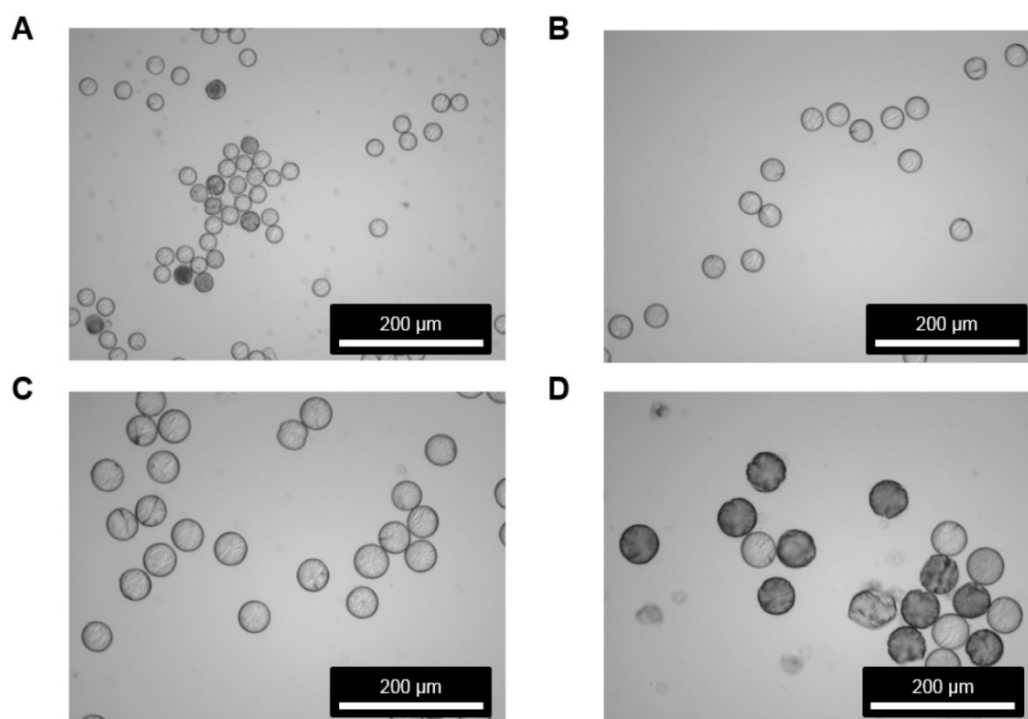


Figure 4. Micrographs of microspheres produced by flow focusing. All samples were produced using the microfluidic chip shown in Figure 1 as per the protocol described in the method section. However, the MS were made of a blend of only two polymers: 1) 97% w/w L-PLA and 2) 3% w/w PEG-PCL. The pictures were acquired by brightfield microscopy. (A) 21.5 ± 1.4 (CV = 6.5%), $Q_{\text{CP}} = 60 \mu\text{L}/\text{min}$, $Q_{\text{DP}} = 1 \mu\text{L}/\text{min}$, [DP] = 10% w/v; (B) 28.8 ± 1.5 (CV = 5.2%), $Q_{\text{CP}} = 30 \mu\text{L}/\text{min}$, $Q_{\text{DP}} = 1 \mu\text{L}/\text{min}$, [DP] = 10% w/v; (C) 42.1 ± 1.7 (CV = 4.1%), $Q_{\text{CP}} = 30 \mu\text{L}/\text{min}$, $Q_{\text{DP}} = 1 \mu\text{L}/\text{min}$, [DP] = 5% w/v; (D) 48.4 ± 2.2 (CV = 4.5%), $Q_{\text{CP}} = 20 \mu\text{L}/\text{min}$, $Q_{\text{DP}} = 1 \mu\text{L}/\text{min}$, [DP] = 40% w/v.

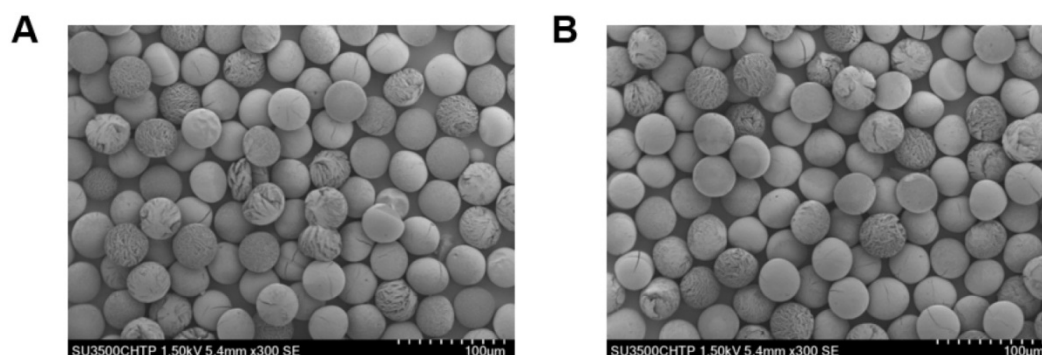


Figure 5. Morphology inspection of microspheres before and after ^{188}Re labeling. Images acquired by SEM are shown for the MS (A) before and (B) after ^{188}Re labeling. For (B), the images were taken after ^{188}Re decay. No morphological changes were observed in the MS after ^{188}Re labeling, as determined by visual inspection.

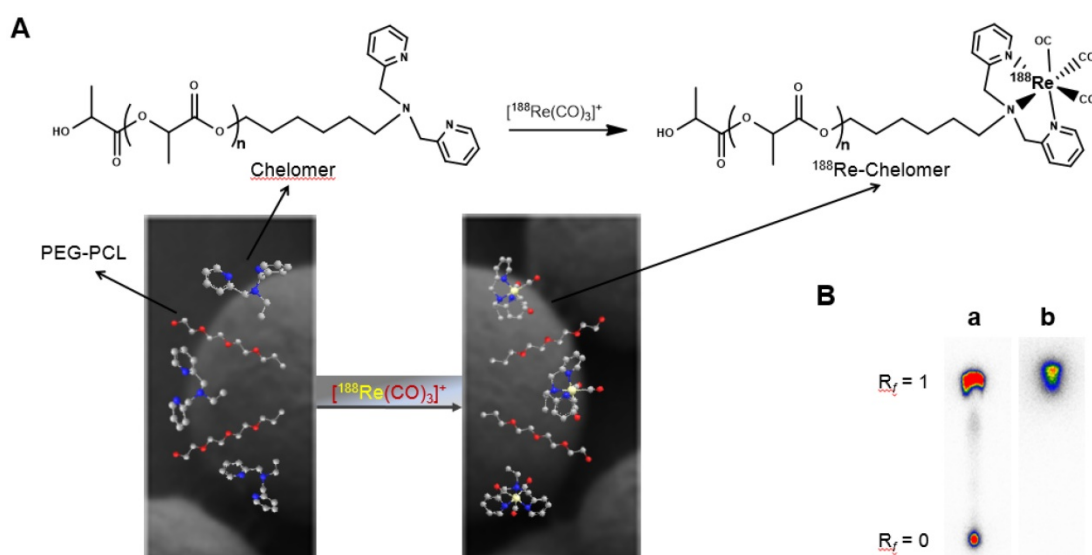


Figure 6. Radiolabeling of the microspheres with ^{188}Re . (A) Top: Metal coordination of the custom-synthesized chelating polymer. Bottom: Cartoon of the surface of a single MS with the chelomer before and after radiolabeling with $[^{188}\text{Re}(\text{CO})_3]^+$. Grey: Carbon, Red: Oxygen, Blue: Nitrogen, Yellow: Rhenium. (B) The pictures show developed TLCs of (a) ^{188}Re -MS and (b) $[^{188}\text{Re}(\text{CO})_3]^+$. The mobile phase was saline. The ^{188}Re -MS stay at $R_f = 0$, but free $[^{188}\text{Re}(\text{CO})_3]^+$ moves to $R_f = 1$.

^{90}Y -MS are difficult to administer homogeneously because of their high density which is 3.3 and 1.6 g/mL for TheraSphere[®] and SIR-Spheres[®], respectively [62]. This causes some of the MS to settle in the lumen of the catheters before and during administration, resulting in a decrease in the number of ^{90}Y -MS administered to the patient. An ideal radioembolization agent should have a density close to the 1.06 g/mL density of blood [20]. ^{188}Re -MS are mainly made of 2.2 kDa L-PLA with a density of 1.2 g/mL [63], a conjugate of L-PLA (i.e., the ^{188}Re chelomer), and another polyester of similar density (i.e., the PCL-PEG). Due to their significantly lower density, ^{188}Re -MS exhibit improved flow dynamics over ^{90}Y -MS. While ^{188}Re -MS still settle in the lumen of the catheters, we showed experimentally that we can prolong the time they remain in suspension by injecting them in a viscous HEC/Dex/CSB solution. Specifically, we measured the optical density, or turbidity, of the 40 μm suspension of non-radioactive MS at 450 nm every 30 s for 1 h using an ultraviolet/visible spectrophotometer (DU 800, Beckman Coulter; Brea, California, United States). As shown in Figure 7, the MS suspended in HEC/Dex/CSB remain in suspension for approximately 10 min.

Our research group has reported in the past that the chelomer used to prepare our ^{188}Re -MS also binds rhenium's congener $^{99\text{m}}\text{Tc}$ [45]. The fact that the same MS can be labeled with either ^{188}Re or $^{99\text{m}}\text{Tc}$ offers exciting opportunities for theranostic applications. The hepatic perfusion study that is conducted prior to radioembolization to assess the degree of portal shunting to the lungs requires imaging $^{99\text{m}}\text{Tc}$ -MAA with a planar 2D scan following a hepatic intra-arterial catheterization. If more than 10% of the

activity injected is found in the lungs, radioembolization is contraindicated. Nevertheless, $^{99\text{m}}\text{Tc}$ -MAA does not have the same density, morphology, and size distribution as ^{90}Y -MS. Therefore, the biodistribution of $^{99\text{m}}\text{Tc}$ -MAA cannot be expected to be identical to ^{90}Y -MS, leading to inaccurate diagnoses [27, 28].

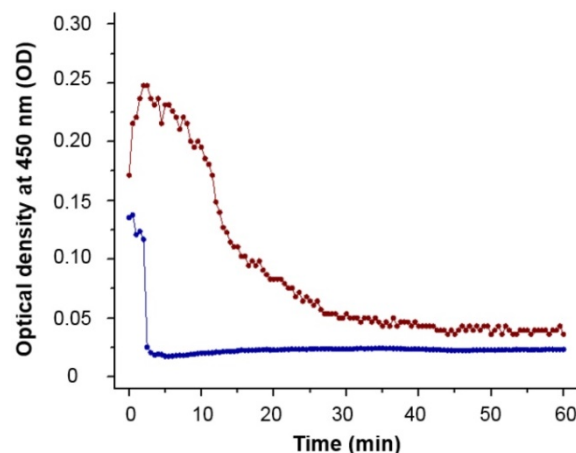


Figure 7. Turbidimetric analysis of $\sim 40 \mu\text{m}$ microspheres. The MS were suspended at a concentration of 2 mg/mL in either saline (blue line) or HEC/Dex/CSB solution (red line). The MS remained in suspension for almost 10 min in HEC/Dex/CSB solution, but they started to precipitate in saline almost immediately (<2 min). Each data point is the mean of three independent measurements.

As reported in Häfeli *et al.* (2010), we have already labeled similar MS with $^{99\text{m}}\text{Tc}$ with a labeling efficiency of 94.7% [45]. These $^{99\text{m}}\text{Tc}$ -MS, which can be easily produced with the same density, morphology, and size distribution to the ^{188}Re -MS, could be imaged by SPECT (or a planar 2D scan) for pre-radioembolization lung shunting assessment and treatment planning, including image-based personalized dosimetry calculations. Then, for radioembolization, identical MS could be labeled with ^{188}Re in

patient-specific activity concentrations, based on the ^{99m}Tc -MS scans. Moreover, the number and the size of MS could be easily adjusted on a case-by-case basis.

Development of a hepatocellular carcinoma-bearing animal model

The gold standard in preclinical studies for radioembolization is the use of 5 kg female New Zealand white rabbits bearing VX2 hepatic tumors. VX2 is a virus-induced papilloma which develops into an aggressive carcinoma in various organs of the rabbits (e.g., liver, rectum, lungs, and kidneys) [64]. The advantages of the VX2-bearing rabbit model are: 1) the blood supply to the VX2 hepatic tumors is almost entirely from the hepatic artery, 2) the hepatic artery is large enough to use the smallest available clinical catheter, and 3) the tumor reaches a size of up to 2 g in 2 weeks [65-67]. Nonetheless, this model has faced criticism because the implantation of VX2 hepatic tumors into the rabbits is challenging. For instance, a donor rabbit is required to grow an initial VX2 hepatic tumor. After excision from the donor rabbit, small sections of the tumor are implanted in the liver of the rest of the rabbits following a laparotomy [68, 69]. Therefore, the rabbits are subjected to a costly and complicated surgical procedure a couple of weeks before radioembolization. Furthermore, most preclinical scanners only fit smaller animals, usually mice and rats.

To overcome these shortcomings, we improved on a Novikoff-bearing rat model [39] by replacing the first laparoscopic surgery for the tumor implantation with an ultrasound-guided tumor cell injection step. For this purpose, a suspension of N1-S1 cells in Matrigel™ was directly injected into the liver of the two rats allocated to Cohort A (HCC/+): R01 and R02. The overall procedure took less than 30 min, from mounting each rat on the operating table to withdrawing the needle after inoculation of the N1-S1 cells. None of the rats experienced any complications during the procedure and recovered fully in the first 15 min following the injection.

Figure 8 depicts sonograms of the different stages of the procedure. The needle can be visualized on the machine's screen and thus the exact site of injection is known. This in turn makes possible to adjust the depth of the injection. We recommend a minimum of 3 to 4 mm in depth to avoid abnormal tissue growth near the surface of the liver. Following the inoculation of the suspension of N1-S1 cells, Matrigel™ begins to polymerize and form a matrix for cell proliferation. This results in a focus of N1-S1 cells at the site of injection which is easily distinguished under ultrasound guidance, providing evidence of the attachment of the N1-S1 cells to the tissue.

The presence of tumors in R01 and R02 was corroborated during necropsy. Post mortem examination revealed that the rats developed a single tumor in the left lateral lobe weighing 0.6 and 0.4 g, respectively. No tumors were found in any other organs. R01 was euthanized 48 h post-radioembolization, whereas R02 was euthanized 2 weeks post-radioembolization.

Radioembolization and quantitative SPECT

The set of catheters described in the methods section allowed for the administration of the suspension of ^{188}Re -MS with minimal losses during the process. No substantial activity was found in the needles and syringes. Losses were only recorded in the pipette tip used to suspend the ^{188}Re -MS in the HEC/Dex/CSB solution. The activity in all these tools, including the vial with the stock of ^{188}Re -MS, was less than 0.7 MBq. This led to the delivery of $96.4 \pm 2.5\%$ of the total activity injected into each rat. The administration of microspheres was also verified by measuring the total activity in each rat's liver on the quantitative SPECT images (Table 1). Overall, differences between dose-calibrator measurements of activities and SPECT images were less than 13%. The suspension of ^{188}Re -MS was easily injected once Catheter 1 was secured at the injection site. Due to the addition of Chicago Sky Blue 6B, the parenteral formulation had a distinctive blue color, facilitating monitoring the flow of ^{188}Re -MS. Each injection was completed in up to 2 min with no difficulties during administration, followed by 150 μL of saline to flush the set of catheters. The administration device was found to be safe, reliable, and effective. Due to its efficiency, this strategy could be transferred to other preclinical studies involving the use of MS, either non-radioactive or radioactive.

While there are no clinical studies that directly compare radioembolization with ^{188}Re and ^{90}Y , a few clinical studies have reported the utilization of ^{188}Re -radiopharmaceuticals for radioembolization [70-73]. Since the energy spectra of ^{188}Re and ^{90}Y 's β^- particles are similar, both radioisotopes deposit a similar radiation dose per unit decay. Due to their difference in half-life, however, the initial injected activity of ^{188}Re must be approximately 3.8 times higher than that of ^{90}Y in order to achieve a comparable dose. For this reason, the biological effectiveness of the two treatments can be expected to be different. The requirement of the higher initial activity in the case of ^{188}Re radioembolization would result in a higher dose rate that rapidly falls off after 24 or 48 h. This may in turn result in an improved tumor response as the probability of inducing DNA damage increases with dose rate. Any complications can be minimized by utilizing a radioembolization

agent that can be selectively delivered to the tumor, maintaining the cumulative dose in the liver below the safety threshold of 70 Gy commonly employed in the clinical setting [74]. Figure 9 shows representative SPECT/CT images of the rats, where it is seen that there is no extrahepatic deposition of ^{188}Re -MS. Due to their size, the ^{188}Re -MS lodged primarily in the liver vasculature of the rats. Figure 10 exemplifies the deposition of a MS in the PHA after ^{188}Re decay, 14 days post-injection of the ^{188}Re -MS. Additionally, the SPECT/CT images revealed that the ^{188}Re -MS accumulated predominantly in the tumor in the two rats of Cohort A (HCC/+), whereas they distributed

evenly throughout the liver in the two rats of Cohort B (HCC/-). R01 and R03 are comparable to each other as the activity injected in each case was similar: 44.5 and 55.5 MBq of ^{188}Re -MS, respectively. Similarly, R02 and R04 are comparable to each other with the following activities injected: 12.6 and 11.5 MBq of ^{188}Re -MS, respectively. The effective half-life of ^{188}Re -MS derived from SPECT-based time-activity curves of R01 and R03 were 16.1 h and 17.6 h, respectively (Figure 11). These measurements, which are approximately equal to the physical half-life of ^{188}Re , indicate that no biological clearance of ^{188}Re -MS nor chemical separation of ^{188}Re from the MS occurred.

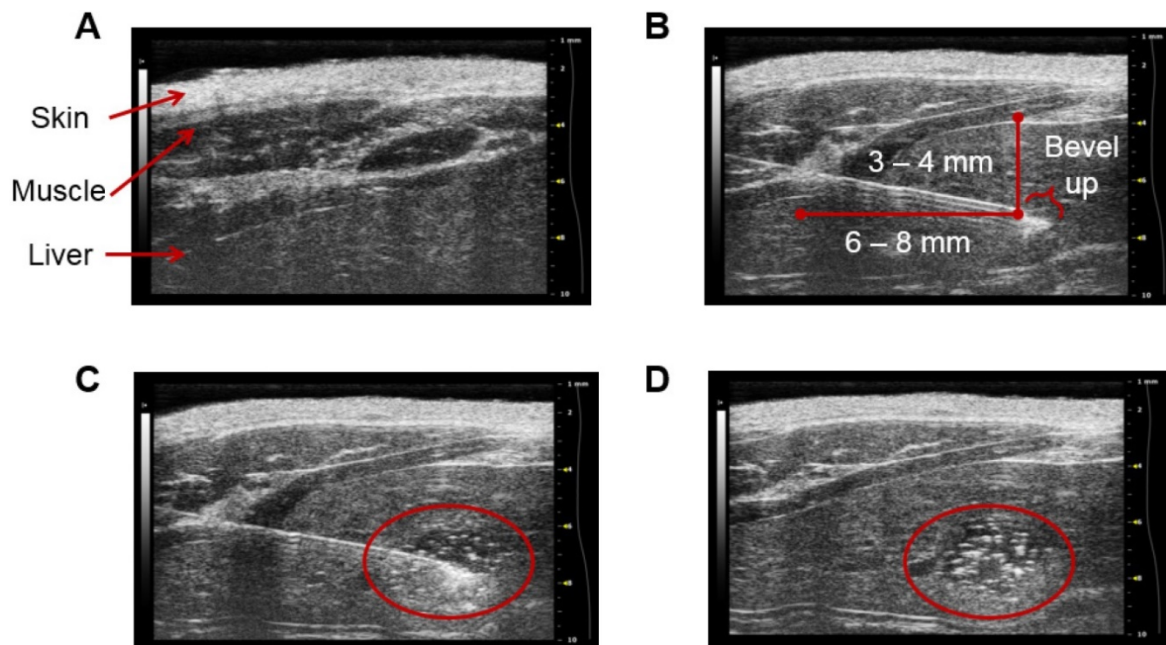


Figure 8. Stages of ultrasound-guided inoculation of NI-S1 cells into the liver. The sonograms were acquired with the Vevo® 2100 Digital Imaging Platform (Visual Sonics; Toronto, Ontario, Canada). The stages of the procedure are: (A) visualization of the liver; (B) insertion of the needle through the skin, the abdominal wall, and the liver; (C) injection of 1×10^6 NI-S1 cells suspended in 50 μL of Matrigel™; and (D) detection of a focus of NI-S1 cells after polymerization of the Matrigel™ (delineated in red). The images correspond to R01. The injection was performed directly into the left lobe of the liver.

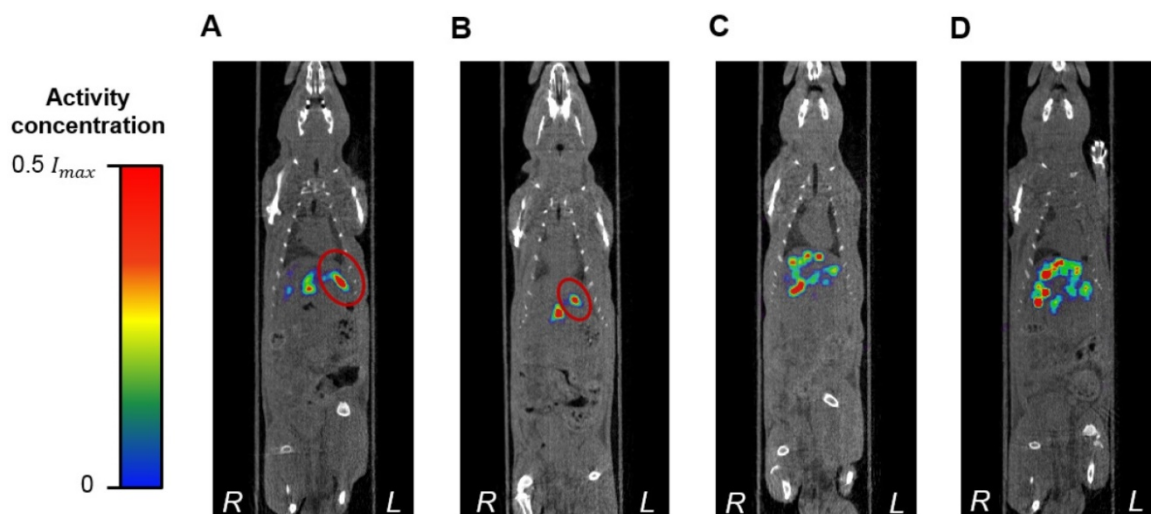


Figure 9. Biodistribution of ^{188}Re -labeled microspheres. Cohort A (HCC/+): (A) R01 and (B) R02. Cohort B (HCC/-): (C) R03 and (D) R04. Representative SPECT/CT images acquired 1 h-post radioembolization of (A) R01 (47,700 ^{188}Re -MS, 44.4 MBq), (B) R02 (47,700 ^{188}Re -MS, 12.6 MBq), (C) R03 (71,600 ^{188}Re -MS, 55.5 MBq), and (D) R04 (47,700 ^{188}Re -MS, 11.5 MBq). For R01 and R02, the tumor is delineated in red. The activity concentration is reported using a relative scale, where I_{max} is the maximum voxel intensity value of each image.

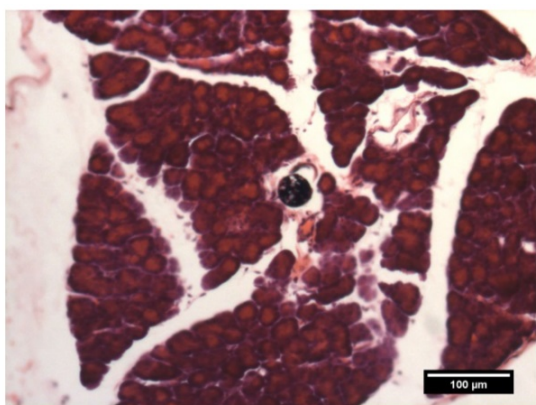


Figure 10. Deposition of a microsphere in the proper hepatic artery. The image shows a transverse H&E stained 50 μm -thick (!) section of the PHA acquired by brightfield microscopy.

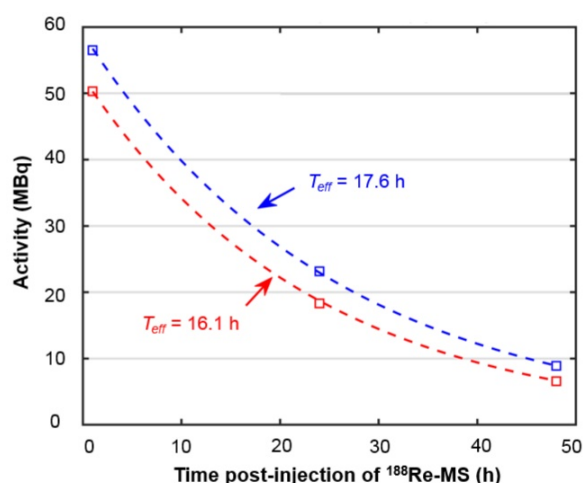


Figure 11. Time activity curves derived from liver activity measurements on the quantitative SPECT images. The graph depicts the time activity curves of R01 (HCC/+) and R03 (HCC/-). The effective half-life was obtained by fitting the data to mono-exponential functions, as described in the dosimetry calculations section.

For the two rats in Cohort A (HCC/+), the T/H as well as the radiation doses to the tumor and the healthy liver tissue are summarized in Table 2. Since the measurements of effective half-life of ^{188}Re in the rats' livers were approximately equal to the physical half-life of ^{188}Re , a value of $T_{\text{eff}} = 17$ h was utilized in Equation 1 to compute the cumulated activity, and therefore, the dose, in all studies. The estimated radiation dose to the tumor was found to be three to six times larger than to the healthy liver tissue. The healthy liver tissue was exposed to less than 20 Gy in both cases. In a previous study, we demonstrated that ^{188}Re SPECT can be used for quantitative measurements, and therefore, image-based dosimetry, in both preclinical and clinical systems, with activity quantification errors below 10% [32]. However, given that the dosimetry method in this study is a simplified tumor/liver model, we expect that the overall errors of the tumor the healthy liver tissue doses might be higher than 10%. However, given that most of the ^{188}Re dose is deposited locally, the use of a spherical

geometry to model these structures might still be an acceptable approximation. Furthermore, this method is much simpler to implement than segmenting the tumor and the healthy liver tissue boundaries on the CT images of the rats, as there was no difference in their contrast. Not only were the ^{188}Re -MS successfully administered into the liver, but they were also taken up avidly by the tumor. After radioembolization with ^{90}Y -MS, 20-70% of the patients experience abdominal pain, cachexia, fever, nausea, and/or emesis. These adverse effects, collectively known as post-radioembolization syndrome, may be caused by deposition of ^{90}Y -MS in the healthy liver tissue [75, 76]. This pilot study has shown that uniformly-sized ~ 40 μm ^{188}Re -MS are preferentially delivered to the tumor while sparing most of the healthy liver tissue. As a result of their narrow size distribution, ^{188}Re -MS may have the potential of reducing the incidence and the severity of the post-radioembolization syndrome.

Table 2. Radiation doses to the tumor and the healthy liver tissue.

Cohort ID	Animal ID	Tumor mass (g)	Liver mass (g)	T/H	Radiation dose (Gy)	
					Tumor	Healthy liver tissue
Cohort A (HCC/+)	R01	0.6	15.2	6.3	104.0	19.6
	R02	0.4	11.8	3.1	22.0	7.6
Cohort B (HCC/-)	R03	N/A	14.7	N/A	N/A	28.5
	R04	N/A	15.4	N/A	N/A	5.8

The dosimetry calculations were performed with Monte Carlo using the dose kernel convolution method. Only SPECT images acquired 1 h post-radioembolization were used for the analysis.

A limitation of this pilot study was the difficulty of the hepatic intra-arterial catheterization. Due to the small blood vessels of the rats, this is a challenging procedure that requires extensive surgical expertise. Only one of the rats, R02, recovered from all these scans and was euthanized 2 weeks post-radioembolization without any complications. The health of the remaining rats, nevertheless, deteriorated over time. They were all euthanized a few days after the surgery. The same outcomes were observed in a previous study conducted by our research group where no ^{188}Re -MS were injected into the rats, suggesting that these complications are related to the invasiveness of the hepatic intra-arterial catheterization. After consultation with clinical veterinarians, it was concluded that future efforts should focus on improving the repair of the ligation sites at the CHA and the GDA with the use of micro-sutures. Additional work should also be conducted to reduce surgery times. Figure 12, in conjunction with the analysis of the effective half-life of the ^{188}Re -MS (Figure 11), shows that the ^{188}Re -MS stay in the liver for up to 72 h following administration, with minimal changes in their localization. Hence, multiple SPECT/CT scans can be omitted in future studies,

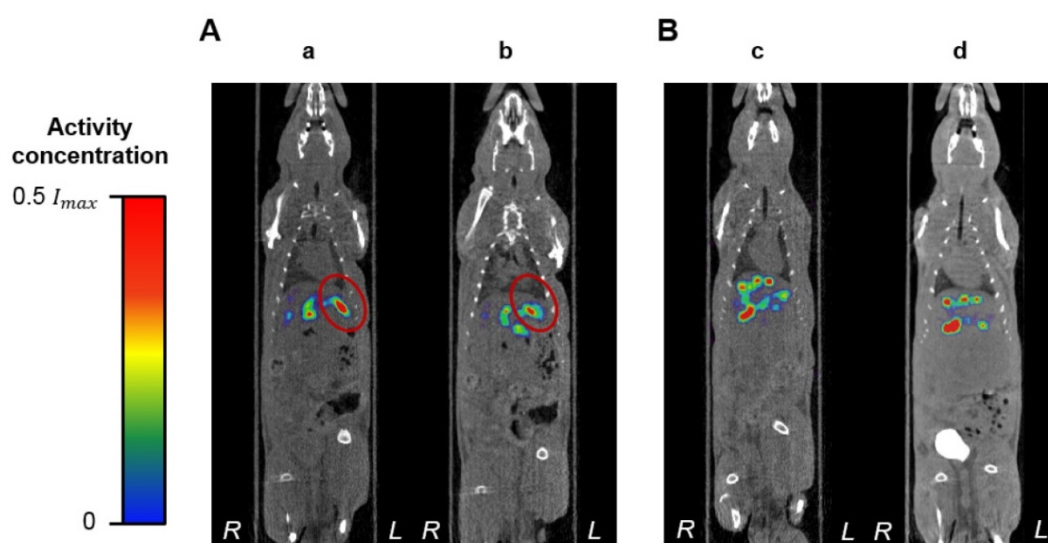


Figure 12. Localization of the ^{188}Re -labeled microspheres over time. Representative SPECT/CT images of (A) R01 ([a] 1 h post-radioembolization and [b] 48 h post-radioembolization). (B) R03 ([c] 1 h post-radioembolization and [d] 72 h post-radioembolization). For R01, the tumor is delineated in red.

potentially helping to speed up the recovery of the rats.

Despite the small sample size, this pilot study provided evidence of the potential application of uniformly-sized and fully biodegradable ^{188}Re -MS in TARE. Given the ease of radiolabeling these MS with ^{188}Re , we were able to adjust the specific activity and the number of MS for each rat. We also estimated the radiation doses to the tumor and the healthy liver using quantities (i.e., T/H) derived from quantitative SPECT, which is valuable information to evaluate the outcomes of the therapy. Following these preliminary results, we are currently designing a long-term study with a larger sample size to investigate the safety and the efficacy of using ^{188}Re -MS for TARE. We are interested in evaluating the effect of the size of our MS on their biodistribution. Specifically, we plan to compare the microembolic effect, or differential deposition in the tumor and the healthy liver tissue, of ^{188}Re -MS with diameters of 20, 30, 40, and 50 μm , which, as shown in this manuscript, have already been produced with the flow focusing microchip described before. Differences in the degree of shunting to the lungs will provide insight into the importance of the size distribution of the MS in TARE.

Conclusion

Uniformly-sized ^{188}Re -MS made primarily from L-PLA, a biodegradable polyester, encompass the next generation of β^- -emitting MS for TARE. Unlike other TARE agents currently available, ^{188}Re -MS have a narrow size distribution and a similar density to blood, which enhances flow dynamics during administration. As ^{188}Re is eluted carrier-free from a $^{188}\text{W}/^{188}\text{Re}$ generator, the MS can be easily labeled

on-site with tuned specific activities. While this is currently a slow two-step process, it will be automated in the future. Using SPECT, the biodistribution of the ^{188}Re -MS can be assessed *in vivo*, allowing for dosimetry calculations. Specifically, it is feasible to calculate the radiation doses to the tumor and the healthy liver tissue. In the clinical setting, this has the potential of allowing for quantitative imaging and accurate patient-specific dosimetry, specifically for the design of treatment plans and the generation of three-dimensional dosimetry maps. A large-scale long-term preclinical study to evaluate the therapeutic efficacy of ^{188}Re -MS with sizes between 20 and 50 μm is currently underway.

Abbreviations

CT: computed tomography; HCC: hepatocellular carcinoma; HEC/Dex/CSB: hydroxyethyl cellulose / dextrose / Chicago sky blue viscous solution; L-PLA: L-poly(lactic acid); MAA: macroaggregated albumin; MS: microspheres; PET: positron emission tomography; PVA: poly(vinyl alcohol); SEM: scanning electron microscopy; SPECT: single photon emission computed tomography; TARE: transarterial radioembolization; TLC: thin layer chromatography.

Acknowledgements

The authors thank all clinical and research staff at the Centre for Comparative Medicine and the Modified Barrier Facility for assistance with animal care and surgical techniques. We also thank Jovan Gill and Nicole Sarden for their help during the ultrasound-guided injections as well as Zeynab Nosrati for help during the administration of ^{188}Re -MS. This research was supported by a collaborative

grant from the Natural Sciences and Engineering Research Council (NSERC) in Canada and the Canadian Institutes of Health Research (CIHR), a discovery grant from NSERC, a grant from the Canada Foundation for Innovation (Grant Number: 25413), and the Lundbeck Foundation, Copenhagen, Denmark. Additionally, Dr. J. C. De La Vega acknowledges the National Council of Science and Technology (CONACYT) of Mexico for financial support through a 4 year Ph.D. scholarship.

Competing Interests

The authors have declared that no competing interest exists.

References

- Stewart BW, Kleihues P. World cancer report. Lyon, France; 2003.
- [Internet] Cancer Society's Steering Committee on Cancer Statistics. Canadian cancer statistics. Dec 22, 2018. <http://www.cancer.ca/en/?region=bc>.
- Ulmer SC. Hepatocellular carcinoma: A concise guide to its status and management. *Postgrad Med.* 2000; 107: 117-24.
- Chuang S-C, Vecchia CL, Boffetta P. Liver cancer: Descriptive epidemiology and risk factors other than HBV and HCV infection. *Cancer Lett.* 2009; 286: 9-14.
- Kumar NB. Assessment of malnutrition and nutritional therapy approaches. In: Kumar NB, Ed. *Nutritional management of cancer treatment effects*: Springer; 2012: p. 256.
- Refaat R, Hassan MS. The relationship between the percentage of lung shunting on Tc-99m macroaggregated albumin (Tc-99m MAA) scan and the grade of hepatocellular carcinoma vascularity. *Egypt J Radiol Nucl Med.* 2014; 45: 333-42.
- Kennedy A, Nag S, Salem R, Murthy R, McEwan AJ, Nutting C, et al. Recommendations for radioembolization of hepatic malignancies using yttrium-90 microsphere brachytherapy: A consensus panel report from the radioembolization brachytherapy oncology consortium. *Int J Radiat Oncol Biol Phys.* 2007; 68: 13-23.
- Salem R, Lewandowski RJ. Chemoembolization and radioembolization for hepatocellular carcinoma. *Clin Gastroenterol Hepatol.* 2013; 11: 604-11.
- Kennedy AS, McNeillie P, Dezarn WA, Nutting C, Sangro B, Wertman D, et al. Treatment parameters and outcome in 680 treatments of internal radiation with resin ⁹⁰Y-microspheres for unresectable hepatic tumors. *Int J Radiat Oncol Biol Phys.* 2009; 74: 1494-500.
- Pasciak AS, Bourgeois AC, Bradley YC. A microdosimetric analysis of absorbed dose to tumor as a function of number of microspheres per unit volume in ⁹⁰Y radioembolization. *J Nucl Med.* 2016; 57: 1020-6.
- McCann JW, Larkin AM, Martino LJ, Eschelmann DJ, Gonsalves CF, Brown DB. Radiation emission from patients treated with selective hepatic radioembolization using yttrium-90 microspheres: Are contact restrictions necessary? *J Vasc Intervent Radiol.* 2012; 23: 661-7.
- Sangro B, Iñarrairaegui M, Bilbao JJ. Radioembolization for hepatocellular carcinoma. *J Hepatol.* 2012; 56: 464-73.
- Murthy R, Nunez R, Szklaruk J, Erwin W, Madoff DC, Gupta S, et al. Yttrium-90 microsphere therapy for hepatic malignancy: Devices, indications, technical considerations, and potential complications. *Radiographics.* 2005; 25: S41-S55.
- Browne E. Nuclear data sheets for A = 90. *Nucl Data Sheets.* 1997; 82: 379-546.
- [Internet] BTG. Package insert for TheraSphere yttrium-90 glass microspheres. Dec 22, 2018. https://btgplc.com/BTG/media/TheraSphere-Documents/PDF/TheraSphere-Package-Insert_USA_Rev-14.pdf.
- Liapi EA, Geschwind JF. Radioembolization for hepatocellular carcinoma. In: Matthew AM, Murphy KPJ, Thomson KR, Venbroux AC, Morgan RA, editors. *Image-Guided Interventions E-Book: Expert Radiology Series*. 2nd ed: Elsevier Health Sciences; 2013. p. 1344.
- [Internet] SirTex. Package insert for SIR-Spheres ⁹⁰Y resin microspheres. Dec 22, 2018. <https://www.sirtex.com/media/155126/ssl-us-13.pdf>.
- Leung WT, Lau WY, Ho SKW, Chan M, Leung NWW, Lin J, et al. Measuring lung shunting in hepatocellular carcinoma with intrahepatic-arterial technetium-99m macroaggregated albumin. *J Nucl Med.* 1994; 35: 70-3.
- Maus S, Buchholz H, Brochhausen C, Schreckenberger M. Microparticles based on biocompatible, biodegradable polymers. Possible surrogates for Y-90 labelled SIR-Spheres? *J Nucl Med Meeting Abstracts.* 2011; 52: 1594.
- Burrill J, Häfeli UO, Liu DM. Advances in radioembolization - embolics and isotopes. *J Nucl Med Radiat Ther.* 2011; 2: 1-6.
- Gates V, Esmail A, Marshall K, Spies S, Salem R. Internal pair production of ⁹⁰Y permits hepatic localization of microspheres using routine PET: Proof of concept. *J Nucl Med.* 2011; 52: 72-6.
- Willowson K, Forwood N, Jakoby B, Smith A, Bailey D. Quantitative ⁹⁰Y image reconstruction in PET. *Med Phys.* 2012; 39: 7153-9.
- Lhommel R, Goffette P, Van den Eynde M, Jamar F, Pauwels S, Bilbao JJ, et al. Yttrium-90 TOF PET scan demonstrates high-resolution biodistribution after liver SIRT. *Eur J Nucl Med Mol Imag.* 2009; 36: 1696.
- Ho CL, Chen S, Cheung SK, Leung YL, Cheng KC, Wong KN, et al. Radioembolization with ⁹⁰Y glass microspheres for hepatocellular carcinoma: significance of pretreatment ¹¹C-acetate and ¹⁸F-FDG PET/CT and posttreatment ⁹⁰Y PET/CT in individualized dose prescription. *Eur J Nucl Med Mol Imag.* 2018; 45: 2110-21.
- Willowson KP, Tapner M, Bailey DL, Team TQI. A multicentre comparison of quantitative ⁹⁰Y PET/CT for dosimetric purposes after radioembolization with resin microspheres. *Eur J Nucl Med Mol Imag.* 2015; 42: 1202-22.
- Kathy W, Dale LB, Clive B. Quantifying lung shunting during planning for radio-embolization. *Phys Med Biol.* 2011; 56: N145.
- Ahmadzadehfar H, Sabet A, Biermann K, Muckle M, Brockmann H, Kuhl C, et al. The significance of ^{99m}Tc-MAA SPECT/CT liver perfusion imaging in treatment planning for ⁹⁰Y-microsphere selective internal radiation treatment. *J Nucl Med.* 2010; 51: 1206-12.
- Uliel L, Royal HD, Darcy MD, Zuckerman DA, Sharma A, Saad NE. From the angio suite to the γ-camera: Vascular mapping and ^{99m}Tc-MAA hepatic perfusion imaging before liver radioembolization - a comprehensive pictorial review. *J Nucl Med.* 2012; 53: 1736-47.
- Singh B. Nuclear data sheets for A = 188. *Nucl Data Sheets.* 2002; 95: 387-541.
- Lambert B, de Klerk J. Clinical Applications of ¹⁸⁸Re-labeled radiopharmaceuticals for radionuclide therapy. *Nucl Med Commun.* 2006; 27: 223-9.
- Esquinas P, Shinto A, Kamaleswaran K, Joseph J, Celler A. Biodistribution, Pharmacokinetics, and Organ-Level Dosimetry for ¹⁸⁸Re-AHDD-lipiodol radioembolization based on quantitative post-treatment SPECT/CT scans. *EJNMMI Phys.* 2018; 5: 30.
- Esquinas P, Uribe C, Gonzalez V, Rodríguez-Rodríguez C, Häfeli U, Celler A. Accuracy of Rhenium-188 SPECT/CT activity quantification for applications in radionuclide therapy using clinical reconstruction methods. *Phys Med Biol.* 2017; 62: 6379.
- Esquinas PL, Rodríguez-Rodríguez C, Carlos De La Vega J, Bokharai M, Saatchi K, Shirmohammad M, et al. ¹⁸⁸Re image performance assessment using small animal multi-pinhole SPECT/PEI/CT system. *Physica Medica: Eur J Med Phys.* 2017; 33: 26-37.
- Shcherbinin S, Grimes J, Bator A, Cwikla JB, Celler A. Three-dimensional personalized dosimetry for ¹⁸⁸Re liver selective internal radiation therapy based on quantitative post-treatment SPECT studies. *Phys Med Biol.* 2014; 59: 119.
- Hambye A, Dobbeleir A, Vervae A, Knapp F. Image quality with rhenium-188 and technetium-99m: Comparative planar and SPECT evaluation in a phantom study and implications for dosimetry. *World J Nucl Med.* 2002; 1: 12-20.
- Boschi A, Uccelli L, Pasquali M, Duatti A, Taibi A, Pupillo G, et al. ¹⁸⁸W/¹⁸⁸Re generator system and its therapeutic applications. *J Chem.* 2014; 2014: 14.
- Pillai MRA, Dash A, Knapp FF. Rhenium-188: Availability from the ¹⁸⁸W/¹⁸⁸Re generator and status of current applications. *Curr Radiopharm.* 2012; 5: 228-43.
- de Goeij JJM, Bonardi ML. How do we define the concepts specific activity, radioactive concentration, carrier, carrier-free and no-carrier-added? *J Radioanal Nucl Chem.* 2005; 263: 13-8.
- Häfeli UO, Casillas S, Dietz DW, Pauer GJ, Rybicki LA, Conzone SD, et al. Hepatic tumor radioembolization in a rat model using radioactive rhenium (¹⁸⁸Re/¹⁸⁸Re) glass microspheres. *Int J Radiat Oncol Biol Phys.* 1999; 44: 189-99.
- Bokharai M, Schneider T, Dutz S, Stone RC, Mefford OT, Häfeli UO. Production of monodispersed magnetic polymeric microspheres in a microfluidic chip and 3D simulation. *Microfluid Nanofluid.* 2016; 20: 6.
- Häfeli UO, Saatchi K, Elischer P, Misri R, Bokharai M, Labiris NRe, et al. Lung perfusion imaging with monosized biodegradable microspheres. *Biomacromol.* 2010; 11: 561-7.
- Bokharai M, Saatchi K, Häfeli UO. A single microfluidic chip with dual surface properties for protein drug delivery. *Int J Pharm.* 2017; 521: 84-91.
- Saatchi K, Häfeli UO. One-pot syntheses, coordination, and characterization of application-specific biodegradable ligand-polymers. *Dalton Transact.* 2007: 4439.
- Schibli R, Schwarzbach R, Alberto R, Ortner K, Schmale H, Dumas C, et al. Steps toward high specific activity labeling of biomolecules for therapeutic application: Preparation of precursor [¹⁸⁸Re(H₂O)₃(CO)₃]⁺ and synthesis of tailor-made bifunctional ligand systems. *Bioconj Chem.* 2002; 13: 750-6.
- Saatchi K, Häfeli UO. Radiolabeling of biodegradable polymeric microspheres with [^{99m}Tc(CO)₃]⁺ and in vivo biodistribution evaluation using microSPECT/CT imaging. *Bioconj Chem.* 2009; 20: 1209-17.
- Collins T. ImageJ for microscopy. *BioTechniques.* 2007; 43: 25-30.
- Huang M, Liu G. The study of innate drug resistance of human hepatocellular carcinoma Bel7402 cell line. *Cancer Lett.* 1998; 135: 97-105.
- Bartkowski R, Berger MR, Aguiar JLA, Henne TH, Dörsam J, Geelhaar GH, et al. Experiments on the efficacy and toxicity of locoregional chemotherapy of liver tumors with 5-fluoro-2'-deoxyuridine (FUDR) and 5-fluorouracil (5-FU) in an animal model. *J Cancer Res Clin Oncol.* 1986; 111: 42-6.

49. Jäger W, Moskalev I, Janssen C, Hayashi T, Awrey S, Gust KM, et al. Ultrasound-guided intramural inoculation of orthotopic bladder cancer xenografts: A novel high-precision approach. *PLoS ONE*. 2013; 8: e59536.
50. Mullen P. The use of matrigel to facilitate the establishment of human cancer cell lines as xenografts. In: Langdon SP, Ed. *Cancer cell culture: Methods and protocols*. Totowa, NJ: Humana Press; 2004. p. 287-92.
51. Fridman R, Benton G, Aranoutova I, Kleinman HK, Bonfil RD. Increased initiation and growth of tumor cell lines, cancer stem cells and biopsy material in mice using basement membrane matrix protein (Cultrex or Matrigel) co-injection. *Nat Protocols*. 2012; 7: 1138-44.
52. Cho YI, Jung JM. New method of hematocrit correction of whole blood viscosity. *Int Commun Heat Mass Transfer*. 2014; 57: 221-7.
53. Ogawa K. Simulation study of triple-energy-window scatter correction in combined Tl-201, Tc-99m SPECT. *Ann Nucl Med*. 1994; 8: 277-81.
54. Jan S, Santin G, Strul D, Staelens S, Assi K. GATE : A simulation toolkit for PET and SPECT. *Phys Med Biol*. 2004; 49: 4543-61.
55. Bhat M. Evaluated Nuclear Structure Data File (ENSDF). *Nucl Data Sci Technol*. 1992: 817-21.
56. Hackley VA. Nomenclature for ceramic particle dispersion systems. Gaithersburg, MD National Institute of Standards and Technology; 1999.
57. Izumida Y, Sugiura S, Oda T, Satake M, Nakajima M. Production of quasi-monodisperse emulsions with large droplets using a micromachined device. *J Am Oil Chem Soc*. 2005; 82: 73-8.
58. Kuo JC, Tazbirkova A, Allen R, Kosmider S, Gibbs P, Yip D. Serious hepatic complications of selective internal radiation therapy with yttrium-90 microsphere radioembolization for unresectable liver tumors. *Asia-Pacific J Clin Oncol*. 2014; 10: 266-72.
59. Hamoui N, Ryu RK. Hepatic radioembolization complicated by fulminant hepatic failure. *Sem Intervent Radiol*. 2011; 28: 246-51.
60. Riaz A, Lewandowski RJ, Kulik LM, Mulcahy MF, Sato KT, Ryu RK, et al. Complications following radioembolization with Yttrium-90 microspheres: A comprehensive literature review. *J Vasc Intervent Radiol*. 2009; 20: 1121-30.
61. Häfeli UO, Roberts WK, Pauer GJ, Kraeft S-K, Macklis RM. Stability of biodegradable radioactive rhenium (Re-186 and Re-188) microspheres after neutron-activation. *Appl Radiat Isotop*. 2001; 54: 869-79.
62. Caine M, McCafferty MS, McGhee S, Garcia P, Mullett WM, Zhang X, et al. Impact of Yttrium-90 microsphere density, flow dynamics, and administration technique on spatial distribution: Analysis using an in vitro model. *J Vasc Intervent Radiol*. 2017; 28: 260-8.e2.
63. Vauthier C, Schmidt C, Couvreur P. Measurement of the density of polymeric nanoparticulate drug carriers by isopycnic centrifugation. *J Nanoparticle Res*. 1999; 1: 411-8.
64. Anayama T, Nakajima T, Dunne M, Zheng J, Allen C, Driscoll B, et al. A novel minimally invasive technique to create a rabbit VX2 lung tumor model for nano-sized image contrast and interventional studies. *PLOS ONE*. 2013; 8: e67355.
65. Wang D, Bangash AK, Rhee TK, Woloschak GE, Paunesku T, Salem R, et al. Liver tumors: Monitoring embolization in rabbits with VX2 tumors – Transcatheter intraarterial first-pass perfusion MR imaging. *Radiology*. 2007; 245: 130-9.
66. Hong K, Khwaja A, Liapi E, Torbenson MS, Georgiades CS, Geschwind J-FH. New intra-arterial drug delivery system for the treatment of liver cancer: Preclinical assessment in a rabbit model of liver cancer. *Clin Cancer Res*. 2006; 12: 2563-7.
67. Hough A, Jr., Seyberth H, Oates J, Hartmann W. Changes in bone and bone marrow of rabbits bearing the VX-2 carcinoma. A comparison of local and distant effects. *Am J Pathol*. 1977; 87: 537-52.
68. Chen JH, Lin YC, Huang YS, Chen TJ, Lin WY, Han KW. Induction of VX2 carcinoma in rabbit liver: Comparison of two inoculation methods. *Lab Animals*. 2004; 38: 79-84.
69. Nass N, Streit S, Wybranski C, Jurgens J, Brauner J, Schulz N, et al. Validation of VX2 as a hepatocellular carcinoma model: Comparison of the molecular reaction of VX2 and HepG2 tumor cells to sorafenib in vitro. *Anticancer Res*. 2017; 37: 87-93.
70. Nowicki ML, Ćwikla JB, Sankowski AJ, Shcherbinin S, Grimes J, Celler A, et al. Initial Study of radiological and clinical efficacy radioembolization using ¹⁸⁸Re-Human Serum Albumin (HSA) microspheres in patients with progressive, unresectable primary or secondary liver cancers. *Med Sci Monitor: Int Med J Exp Clin Res*. 2014; 20: 1353-62.
71. Bernal P, Raoul J-L, Vidmar G, Sereegotov E, Sundram FX, Kumar A, et al. Intra-arterial rhenium-188 lipiodol in the treatment of inoperable hepatocellular carcinoma: Results of an IAEA-sponsored multinational study. *Int J Radiat Oncol Biol Phys*. 2007; 69: 1448-55.
72. Liepe K, Brogssitter C, Leonhard J, Wunderlich G, Hliscs R, Pinkert J, et al. Feasibility of high activity rhenium-188-microsphere in hepatic radioembolization. *Japan J Clin Oncol*. 2007; 37: 942-50.
73. Lambert B, Bacher K, Defreyne L, Gemmel F, Van Vlierberghe H, Jeong JM, et al. ¹⁸⁸Re-HDD/Lipiodol therapy for hepatocellular carcinoma: A phase I clinical trial. *J Nucl Med*. 2005; 46: 60-6.
74. Chiesa C, Mira M, Maccauro M, Romito R, Spreafico C, Sposito C, et al. A dosimetric treatment planning strategy in radioembolization of hepatocarcinoma with ⁹⁰Y glass microspheres. *Quat J Nucl Med Mol Imag*. 2012; 56: 503-8.
75. Peker A, Çiçek O, Soydal Ç, Küçük NÖ, Bilgiç S. Radioembolization with yttrium-90 resin microspheres for neuroendocrine tumor liver metastases. *Diagnos Intervent Radiol*. 2015; 21: 54-9.
76. Riaz A, Awais R, Salem R. Side effects of yttrium-90 radioembolization. *Front Oncol*. 2014; 4: 198.